Polish Society of Composite Materials
Polskie Towarzystwo Materiałów Kompozytowych

24: 2 (2024) 130-140

COMPOSITES THEORY AND PRACTICE

ISSN (online): 2299-128X

Saadia Attou[1], Farida Bouafia[1,2]*, Boualem Serier[2]

[1] *University of Ain Temouchent, Mechanical Engineering Department, Ain Temouchen 46000, Algeria*
[2] *University of Sidi Bel Abbes, LMPM, Mechanical Engineering Department, Sidi Bel Abbes 22000, Algeria*
**Corresponding author. E-mail: farida.bouafia@univ-temouchent.edu.dz*

Received (Otrzymano) 24.02.2023

FINITE ELEMENT ANALYSIS OF STRESS INTENSITY FACTORS OF CRACKS INITIATED IN MULTI-MATERIALS

https://doi.org/10.62753/ctp.2024.08.2.2

In the present work, the finite element method was used to investigate residual stresses in multi-material systems during fabrication. A three-dimensional numerical model was designed to examine the impact of defects at the metal-ceramic interface. Additionally, this model facilitates the analysis of crack behavior originating in ceramic materials. The study extends its scope to explore the effects of crack-interface interaction, crack-defect interaction, and crack size on stress intensity factors.

Keywords: finite element method, crack, defect, metal-ceramic interface

INTRODUCTION

Metal-ceramic bi-materials offer superior properties over conventional alloys and have been widely studied because of their many potential applications. Ceramics such as zirconia, silicon carbides, silicon nitrides, and alumina find a great number of applications in the field of mechanics and thermo-mechanics [1]. Alumina (Al_2O_3) is a popular ceramic material because of its various properties, including high strength, high resistance to wear and corrosion, and high electrical insulation [2]. However, due to its high brittleness and poor processing performance, this ceramic material used alone is not enough to meet the requirements of the engineering field [3]. Many applications of Al_2O_3 require combining it with metals. For instance, the application of Al_2O_3 in electronic device packaging involves combining Al_2O_3 with Cu [4]. In many structural applications, ceramics are selected for critical components forming parts of a total system that is largely metallic, and therefore depend for their success on the fabricator being able to provide good quality ceramic-metal bonds [5]. Various ceramic-to-metal bonding techniques have been developed and improved over the past 50 years [6], for instance, brazing, diffusion bonding, reactive air brazing, glass bonding, and so on [7]. The mechanical properties of solid-state bonded Ni-Al_2O_3 interfaces have been investigated as a function of several bonding parameters (temperature, pressure, and time) and the purity of the starting alumina. It has been shown that they depend upon the plastic deformation of the metal, on the damage induced on the ceramic surface, and on both the nature and amount of interfacial phase that appears during the bonding process [8]. In general, ceramics and metals are bonded at a high temperature [9]. Making a metal-ceramic bond involves inevitable residual stresses when the bonded assembly cools from the bonding temperature to room temperature. These stresses influence the strength and fracture energy of the bond [10]. Residual stresses are generated during fabrication because of discontinuity in the thermal and/or elastic properties of the bonded materials. Metals generally are softer than ceramics and have higher coefficient of thermal expansions [11]. The large mismatch in the coefficient of thermal expansion (CTE) between ceramics and metals results in residual tensile stresses in the brittle ceramic substrates, which drastically reduces the strength of dissimilar bonds [12]. Residual stresses have significant effects on the mechanical stability of the interface since they may cause plastic deformations on the metal side and cracking in the ceramic [13]. The behavior of cracks is studied in terms of variation in the stress intensity factor in Modes I and II [14]. Many analytical and numerical approaches have already been carried out to estimate the residual stresses within ceramic-metal assemblies. To define the mechanical strength of such structures, it is important to estimate these residual stresses [15].

In this study, different cases are analyzed with an attempt to use the finite element method to model ceramic-metal assemblies under thermo-mechanical

loading, along with the effect of the presence of an interface defect and cracks on the fracture behavior of a bi-material. The stress intensity factor parameter is also studied in both modes (Mode I and Mode II) by varying the position and size of the cracks in both directions from the defect.

FINITE ELEMENT MODEL

We analyzed by means of the finite element method the effect of thermomechanical loading applied to two structures consisting of three different materials, Al_2O_3/Ni/Al_2O_3 and Al_2O_3/Ni/HAYNES^{TM}214, on the level and distribution of stresses induced in these constituents in the vicinity of their interfaces. The geometric characteristics of the structures are length (L = 15 mm), width (w = 15 mm), and thickness (e1, e2 and e3), such that e1 = e3 = 5 mm, e2 (nickel thickness) = 0.2 mm. The plate was subjected to a tension load uniformly distributed with P = 16 MPa (see Fig. 1b). The diameter of the interface defect is 1 mm. This defect is located at the alumina interface with a well-defined size. The mechanical characteristics of the materials are: alumina with Young's modulus E = 375 GPa, Poisson's ratio v = 0.28 and coefficient of thermal expansion α = 6.9 e^{-6}; nickel with Young's modulus E = 205 GPa, Poisson's ratio v = 0.29 and coefficient of thermal expansion α = 13.1 e^{-6}; HAYNES^{TM}214 with a Young's modulus E = 218 GPa, Poisson's ratio v = 0.3, and coefficient of thermal expansion α = 13.1 e^{-6}. In the presence of a defect at the ceramic interface, the structure was meshed with a 10-node quadratic tetrahedron (C3D10) element (see Fig. 1c) with a total of 84872 elements.

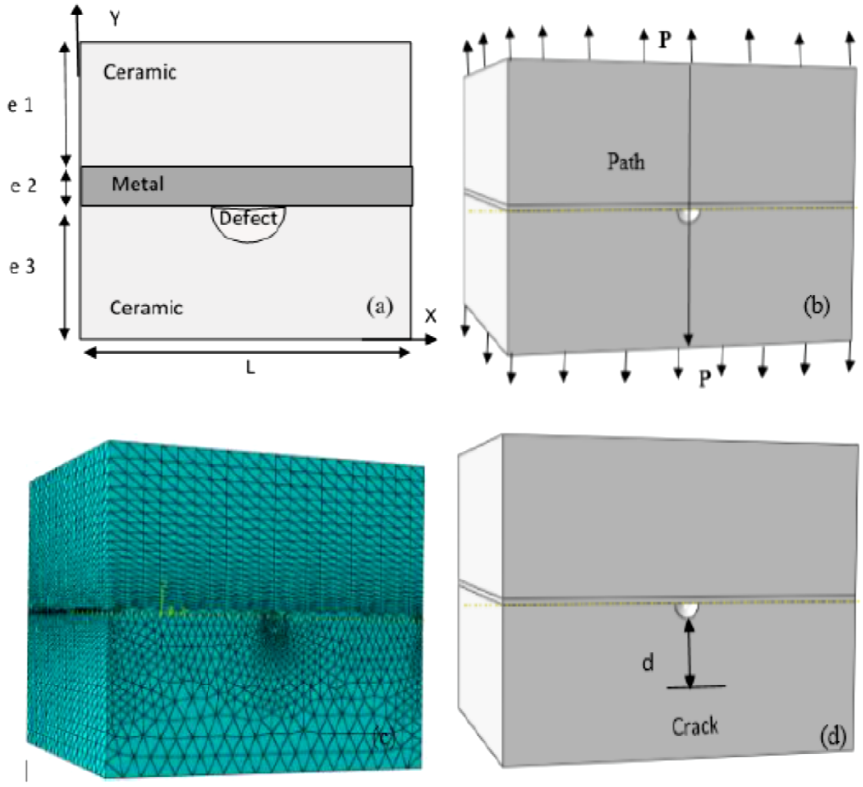

Fig. 1. 2D diagram of metal/ceramic with site of interface defect (a), boundary conditions and loading conditions (b), finite element mesh (c), site of interface crack-defect interaction (d)

RESULTS AND DISCUSSION

Stress distribution

Figure 2 presents the distribution of normal and von Mises equivalent stresses in the three components of the assembly. The normal stresses induced along the x-direction are strongly concentrated in the metal material. These stresses are exerted intensively by nickel in the vicinity of its contact with the ceramics (see Fig. 2b). The stresses developed along the z-direction are on the same level and their distribution is comparable to those of the σxx stresses (see Fig. 2d). The stress generated along the Y direction, which is the axis of mechanical loading application, is at a lower level than the other two normal stresses; this stress is concentrated in the vicinity of the interface, near the edge of the assembly (see Fig. 2c). The von Mises equivalent stress is highly concentrated in the metal and in the vicinity of the metal-ceramic interface as Figure 1a shows. The illustrations of the results in Figure 2 show that the metal-ceramic interface is a site of high-stress concentration.

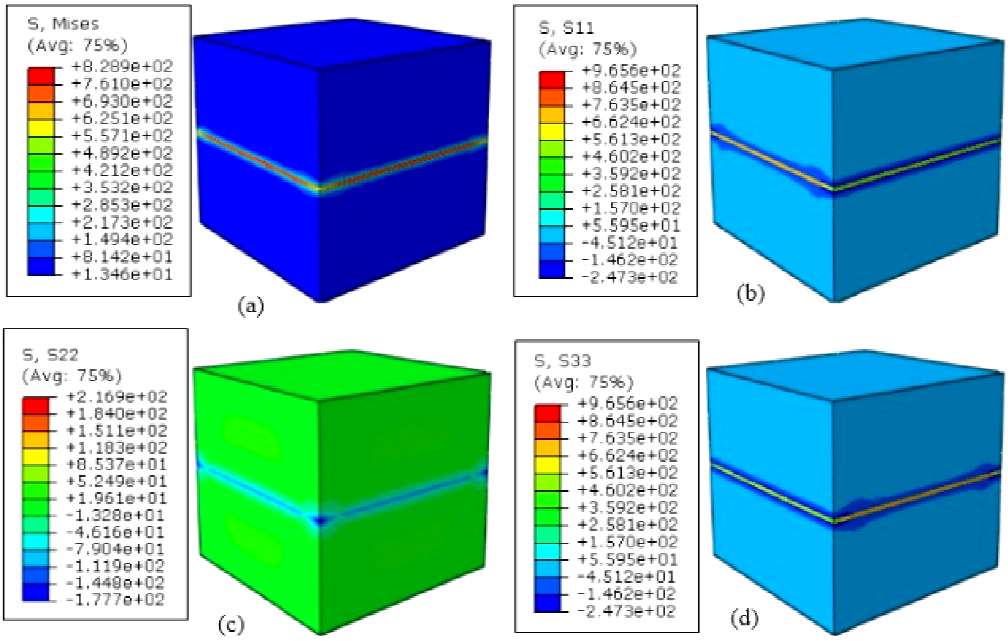

Fig. 2. Von Mises equivalent and normal stress distributions under thermomechanical loading: $P = 16$ MPa, $\Delta T = 500$ °C ($Al_2O_3/Ni/Al_2O_3$)

Effect of temperature

Figure 3 shows the variation in the normal and von Mises equivalent stresses for the alumina/nickel/alumina assembly as a function of the distance and according to the thermomechanical load. The residual stresses generated along the x and z directions compress the ceramic material, while causing tension in the metal near the interface. Far away from the interface, these stresses diminish progressively until they are completely nullified. An increase in temperature leads to a rise in the amplitude of residual stresses.

Nevertheless, the stresses developed along the Y direction are of lower intensity. These stresses compress the multi-material in the vicinity of the interface, near the edge of the structure. The von Mises stresses are strongly concentrated in the metal material and their intensity holds more importance than those for the normal stresses (see Fig. 3a). The intensity of the von Mises stresses increases with the rise in the temperature. The analyses in Figure 3 clearly show that the intensity of the residual stress grows with the increment in thermal loading.

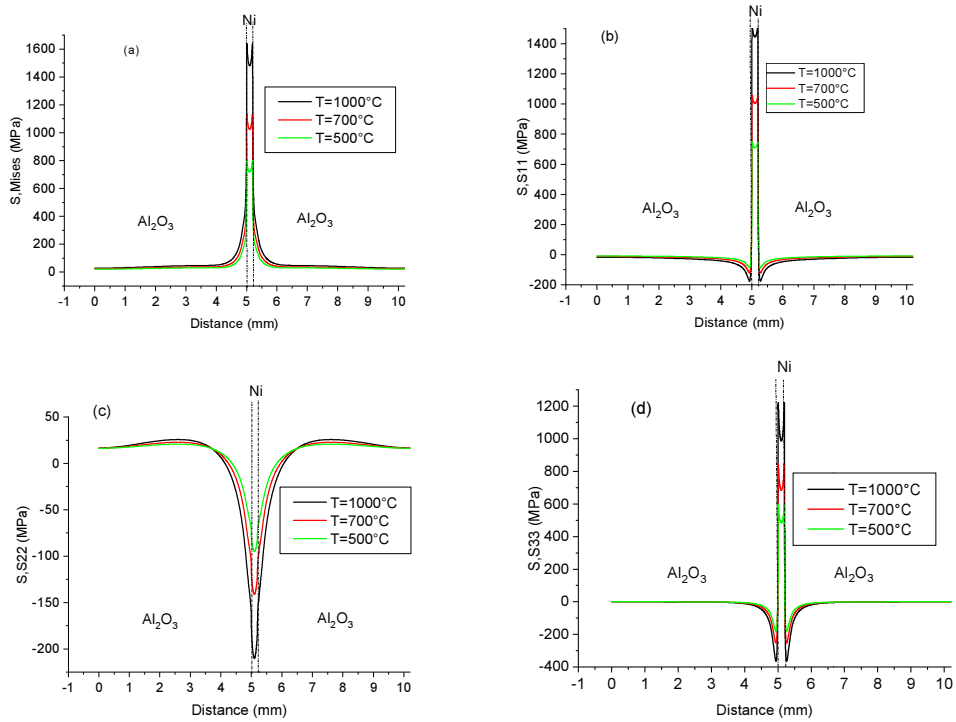

Fig. 3. Variation in von Mises equivalent stress and normal stresses according to thermomechanical loading ($Al_2O_3/Ni/Al_2O_3$)

Stress distribution

The most significant stresses induced in the multi-material along the x-direction are located in the metal near its interface with the ceramic and the alloy. These higher-level stresses compress the ceramic near the interface and cause expansion in the metal and the alloy as shown in Figure 4b. The stresses that developed along the y-direction in the assembly are concentrated on the ceramic and HAYNES^{TM}214 alloy near the interface with nickel. The level of these stresses decreases as one moves away from the interface (see Fig. 4c). In the third direction, z, the normal stresses are of an amplitude comparable to those of the σxx stresses (see Fig. 4d).

The results show that the normal σxx stresses primarily affect the width of the structure, while the σzz stresses primarily affect the thickness. Figure 4a presents the level and distribution of the von Mises equivalent stress induced during the production of the multi-material; this figure shows that the metal-ceramic interface is the site of high stress concentration.

Effect of temperature

The results of the von Mises equivalent stress show that the multi-materials developed at high temperatures raise the residual stresses in the three materials. These constraints are strongly localized at the interfaces (see Fig. 5a). The stresses generated along the x-direction set the ceramic in compression and the alloy in tension on the free edge of the bond. As we move away from the edge, these stresses change signs. It can be inferred that the ceramic is in tension and the alloy in compression. The intensity of these stresses increases as the bonding temperature is augmented (see Fig. 5b). The stresses developed along the y-axis are strongly in tension in the ceramic, while they are in compression in the alloy. As Figure 5c illustrates, a rise in temperature leads to growth in the intensity of stresses. The stresses generated along the z-direction set the ceramic in compression and the alloy in tension in the vicinity of the interface; far away from the interface these stresses diminish progressively until they are completely nullified (see Fig. 5d).

Case of interfacial defect

The distribution of normal and equivalent stresses near the interface defect is shown in Figure 6. The stress generated along the x-direction is highly concentrated in the metal near the edge of the bond (see Fig. 6b). The stresses generated along the y-axis are strongly concentrated on the alumina-nickel interface around the defect (see Fig. 6c). The distribution of the stress developed along the z-direction is comparable to that induced along the first axis (x-axis) of the assembly. Additionally, significant stresses are concentrated in the vicinity of the interface defect (see Fig. 6d). The von Mises equivalent stress is at a much higher level than other normal stresses, which are highly concentrated on the metal and ceramic in the vicinity of the defect as shown in (Fig. 6a). The defect is at a special place of stress concentration as shown in Figure 6.

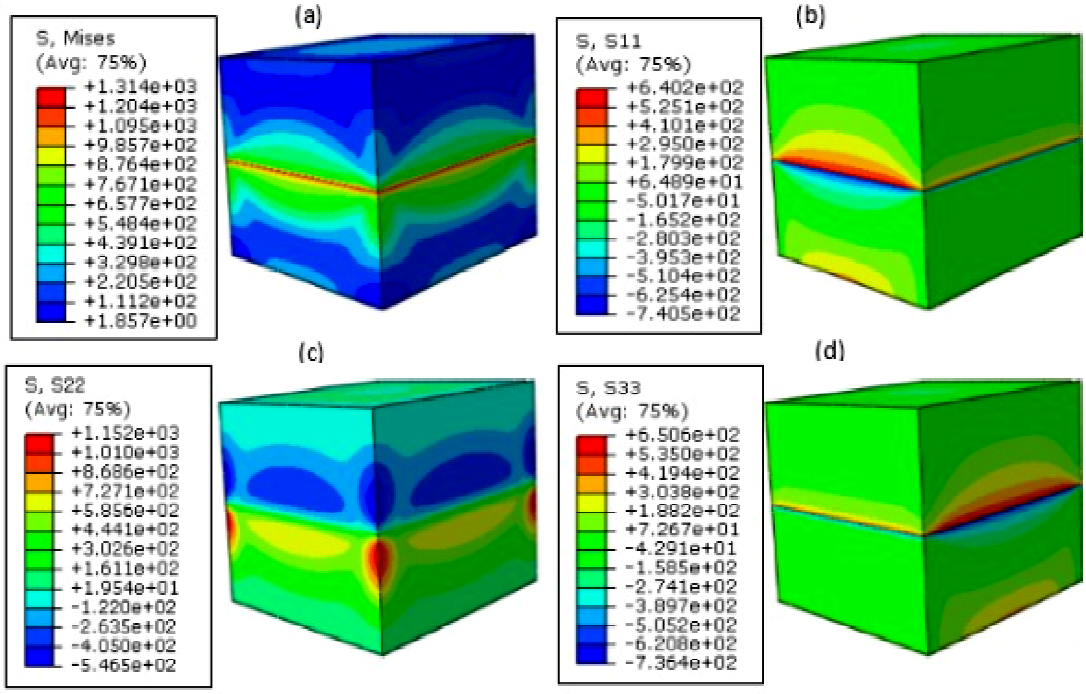

Fig. 4. Von Mises equivalent and normal stress distribution under thermomechanical loading: $P = 16$ MPa, $\Delta T = 500$ °C (HAYNES^{TM}214/Ni/Al_2O_3)

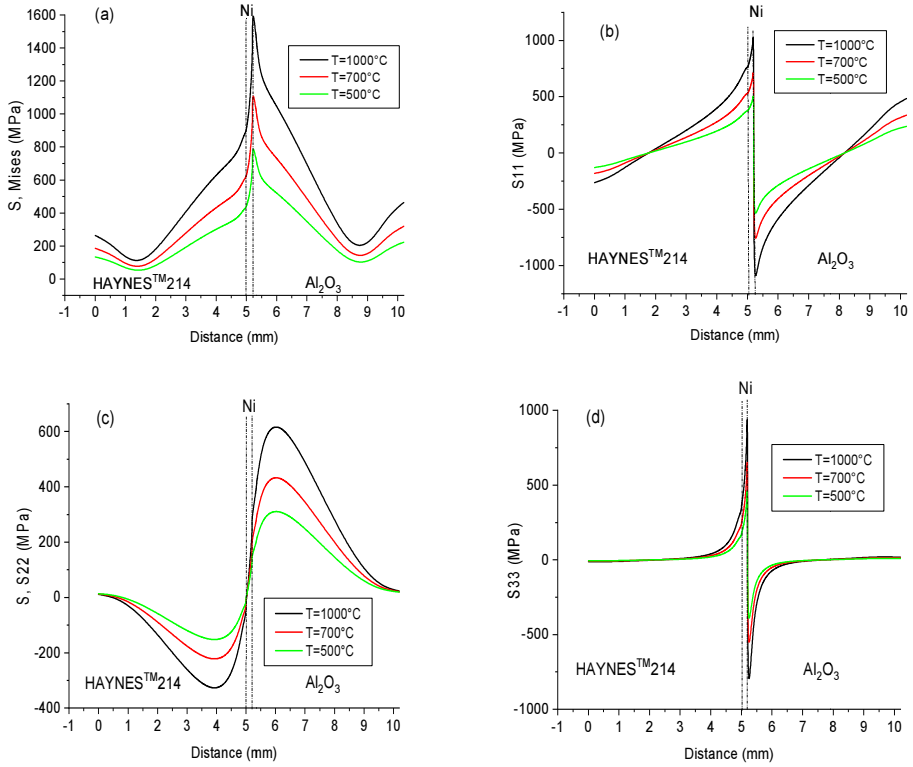

Fig. 5. Variation in von Mises equivalent stress and normal stresses according to thermomechanical loading (HAYNES^{TM}214/Ni/ Al_2O_3)

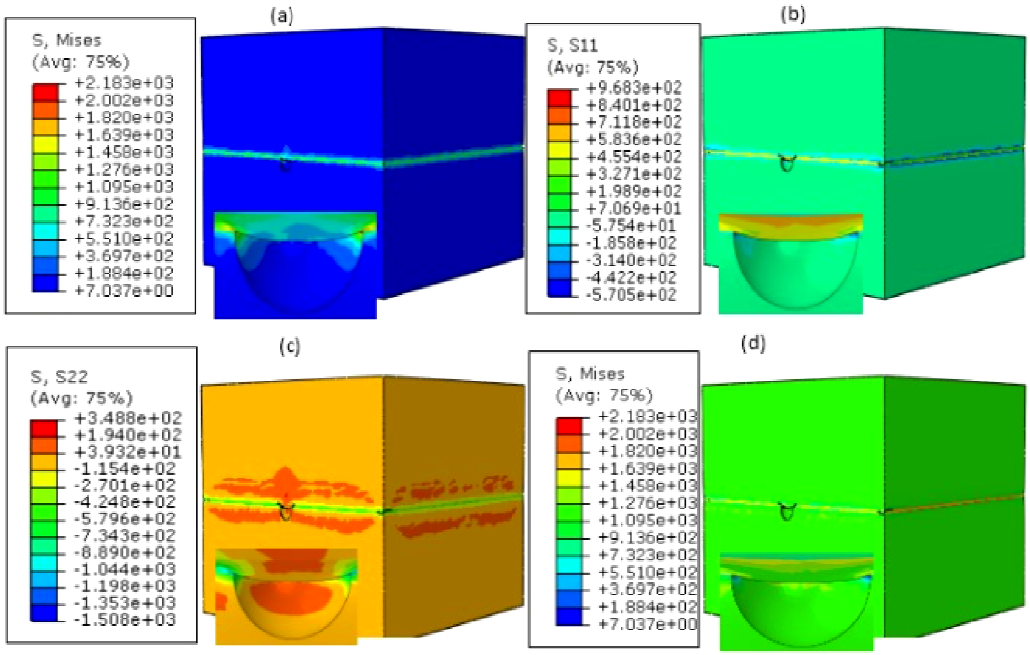

Fig. 6. Variation in von Mises equivalent stress and normal stresses according to thermomechanical loading (HAYNES^{TM}214/Ni/Al_2O_3)

Effect of temperature

Thermal loading sets the defect in tension along the x and z directions (see Figs. 7b and d). The compression becomes higher when the temperature rises. The stresses along the y-direction are lower than the other two axes of the structure (see Fig. 7c); these stresses compress the defect. The von Mises equivalent stresses are heavily concentrated around the interfacial defects; these stresses grew with the increase in temperature (see Fig. 7a).

The illustrations of the results in Figure 7 clearly show that these stresses are strongly concentrated around the interfacial defects. The effects of the interfacial defects grow with increasing thermal loading.

Figure 8 presents the distribution of normal and von Mises equivalent stresses in the HAYNES^{TM}214/Ni/ Al_2O_3 assembly. The normal stress induced along

the x-direction significantly affects the ceramic and alloy near their contact with nickel. The most critical stresses are concentrated at the metaxl-defect interface. The stresses developed along the y-direction are heavily concentrated around the defect; its lowest level is reached at both ends of the bond as shown in Figure 8c. The stresses induced along the z-direction are almost comparable to those induced along the first axis (x-axis). However, the stress generated along the x-axis primarily affects the length, whereas the stress along the z-axis primarily affects the width. The von Mises stresses are highly concentrated in the ceramic and alloy HAYNES^{TM}214 near the edge of its interface with nickel. The presence of defects on the surface of the ceramic plays a leading role in stress concentration.

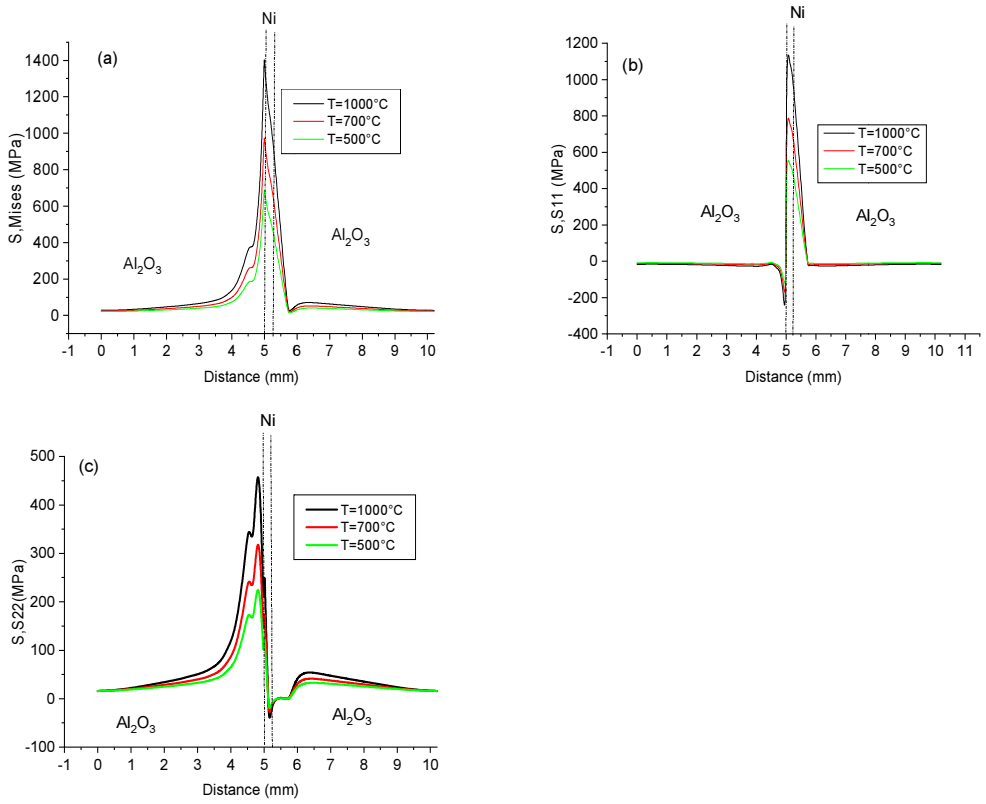

Fig. 7. Variation in von Mises equivalent and normal stress of a multi-material with a defect (Al_2O_3/Ni/Al_2O_3)

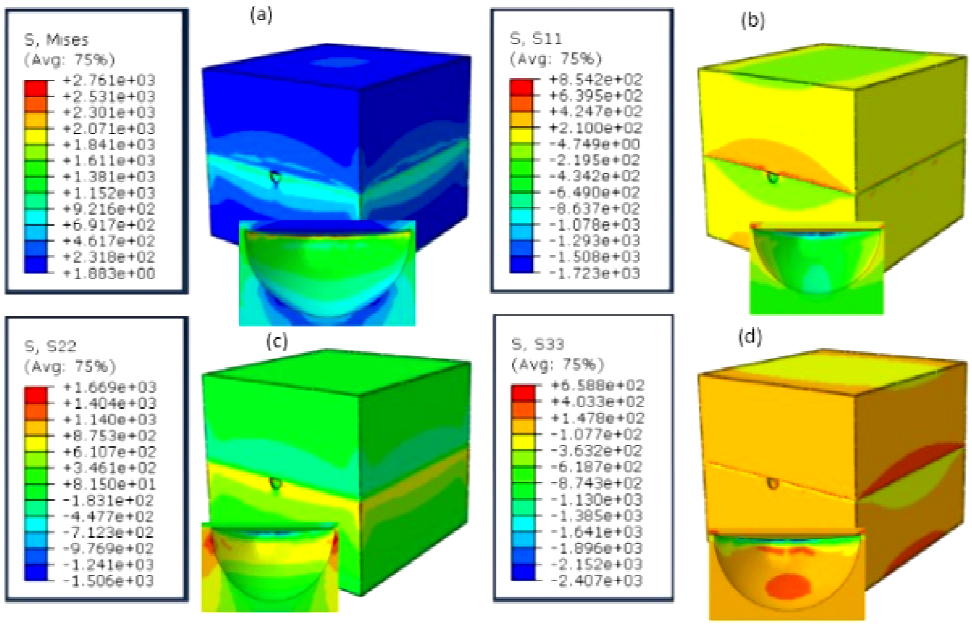

Fig. 8. Von Mises equivalent and normal stress distribution in multi-material with interfacial defect for P = 16 MPa, T = 500 °C (HAYNES^{TM}214/Ni/Al_2O_3)

Effect of temperature

The von Mises equivalent stress sets the whole structure in tension; the effects of the interfacial defects grow with increased thermal loading. The stresses generated in the X direction are at a much higher level near the defect; these stresses are in compression in the ceramic and tension in the alloy on the free edge of the bond. In contrast, away from the edge these stresses set the ceramic in tension and the alloy in compression. The variation in normal stresses σyy set the ceramic in tension and the alloy in compression in the vicinity of the interface. The stresses generated in direction z of the structure are strongly concentrated near the interfaces, the most important being near the defect.

This type of stress compresses the defect; the compression becomes higher when the temperature is increased. The analyses of Figure 9 show that the presence of defects on the surface of the ceramic plays a leading role in stress concentration, and the intensity of these stresses grows as the thermal load increases.

Comparison

Figures 10a and b present the variation in the normal stress induced along the y-direction in the Al_2O_3/Ni/Al_2O_3 and HAYNES^{TM}214/Ni/Al_2O_3 structures. These figures clearly show that the presence of a defect at the interface induces greater stresses and the site of the interface defect is a significant site of stress concentration.

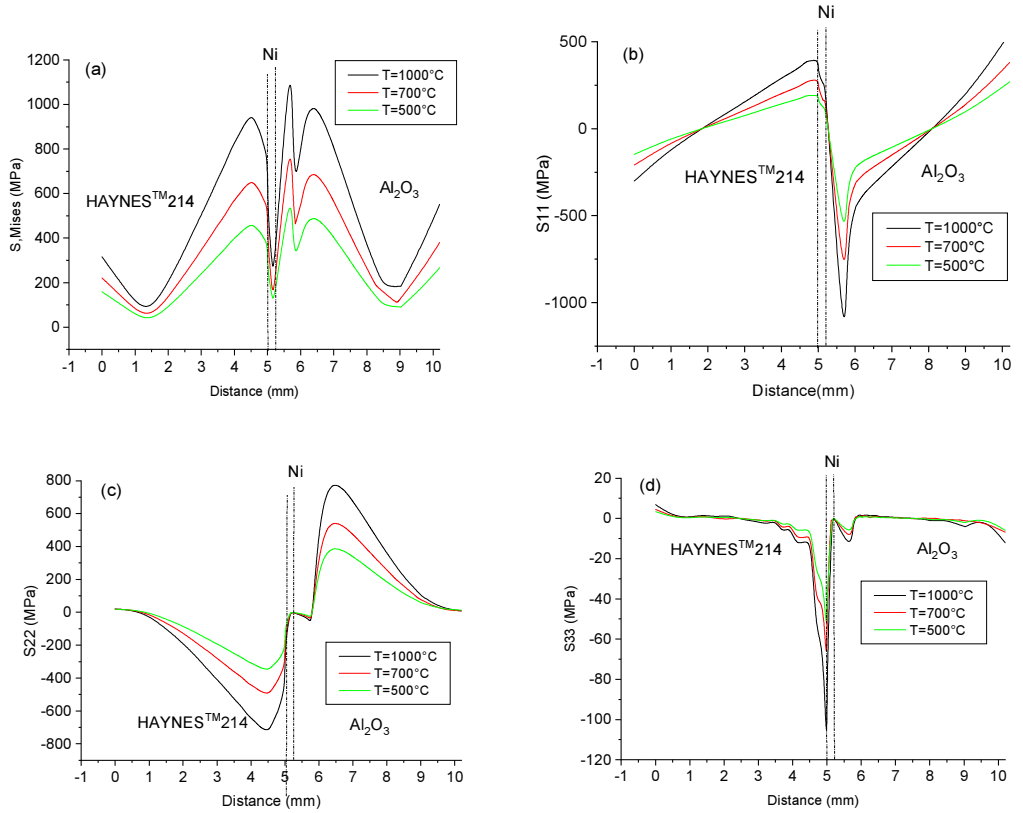

Fig. 9. Variation in von Mises equivalent and normal stress of multi-material with defect (HAYNES^{TM}214/Ni/Al_2O_3)

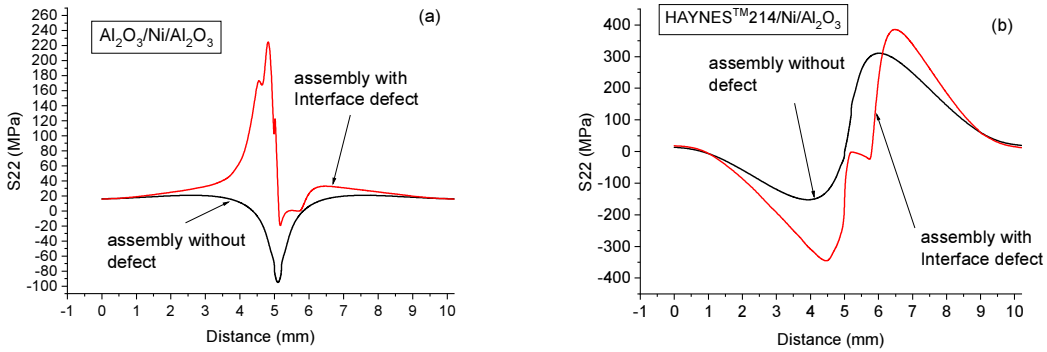

Fig. 10. Comparison of variation in normal stress σ_{yy} in two models under thermomechanical loading T = 500 °C, P = 16 MPa

Stress intensity factors

The position of the crack relative to the interface on the stress intensity factor is analyzed below. The effect of the distance between the interface and the crack on the stress intensity factor is given in Figure 11; this position is defined by d. The rupture in Mode I in the symmetric assembly grows as the distance between the crack and the interface increases as in seen in Figure 11a. In contrast to the second assembly, HAYNES^{TM}214/Ni/Al_2O_3, the presence of the crack near the interface leads to augmentation in these factors (see Fig. 11c). This clearly indicates that the residual stresses are heavily localized in the vicinity of the interface, which explains the significant propagation of this crack. The rupture factors in Mode II are practically negligible as compared to the rupture factors in Mode I. The illustrations of the in Figure 11 show that the values of SIF decrease when the assembly is symmetric, while the risk of propagation is the greatest when the crack is initiated near the interface of the second assembly.

Figure 12 shows the variation in the stress intensity factor as a function of the distance between the crack and the interface defect along the x-axis. The stress intensity factor in Mode I grows as the distance between the crack and the defect decreases. We can explain the negative values in the symmetric assembly, in that the crack is in a compression stress field when the crack is tangent to the defect, and the intensity factor reaches the maximum value. The rupture in Mode II in the first assembly is almost negligible (see Fig. 12b), while in the second assembly it is more important; it grows as the distance between the crack and defect increases (see Fig. 12d).

The variation in the stress intensity factor as a function of the crack-defect interaction along the y-axis is shown in Figure 13. The rupture in Mode I in the symmetric assembly grows as the distance between the crack and the interfacial defect increases (see Fig. 13a) and the rupture in Mode II is almost negligible (see Fig. 13b). In contrast, the rupture in Mode I in the second assembly grows as the distance between the defect and crack decreases and its value is more important compared to the rupture in the symmetric assembly; additionally, its intensity is more important than the intensity of the first assembly (see Fig. 13c). SIF in Mode II rises as the distance between the crack and the defect increases.

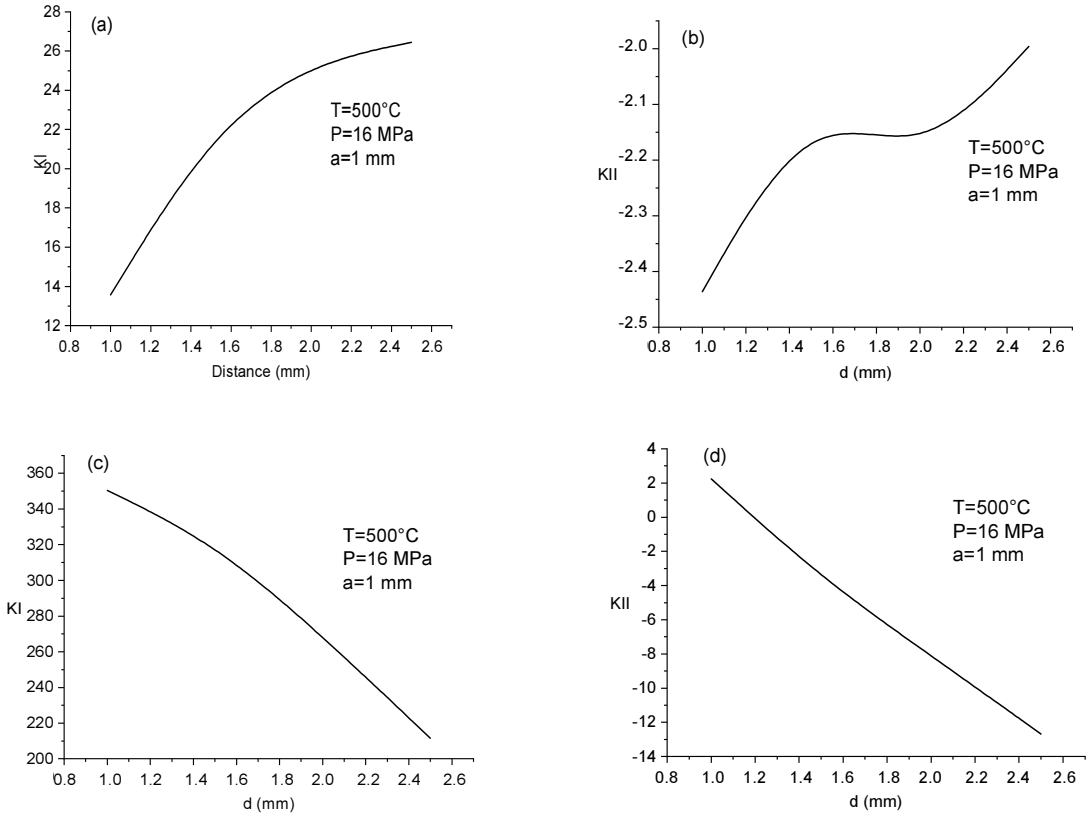

Fig. 11. Variation in stress intensity factor as function of crack-interface interaction: a) Mode I in Al_2O_3/Ni/Al_2O_3, b) Mode II in Al_2O_3/Ni/Al_2O_3, c) Mode I in HAYNES^{TM}214/Ni/Al_2O_3, d) Mode II in HAYNES^{TM}214/Ni/Al_2O_3

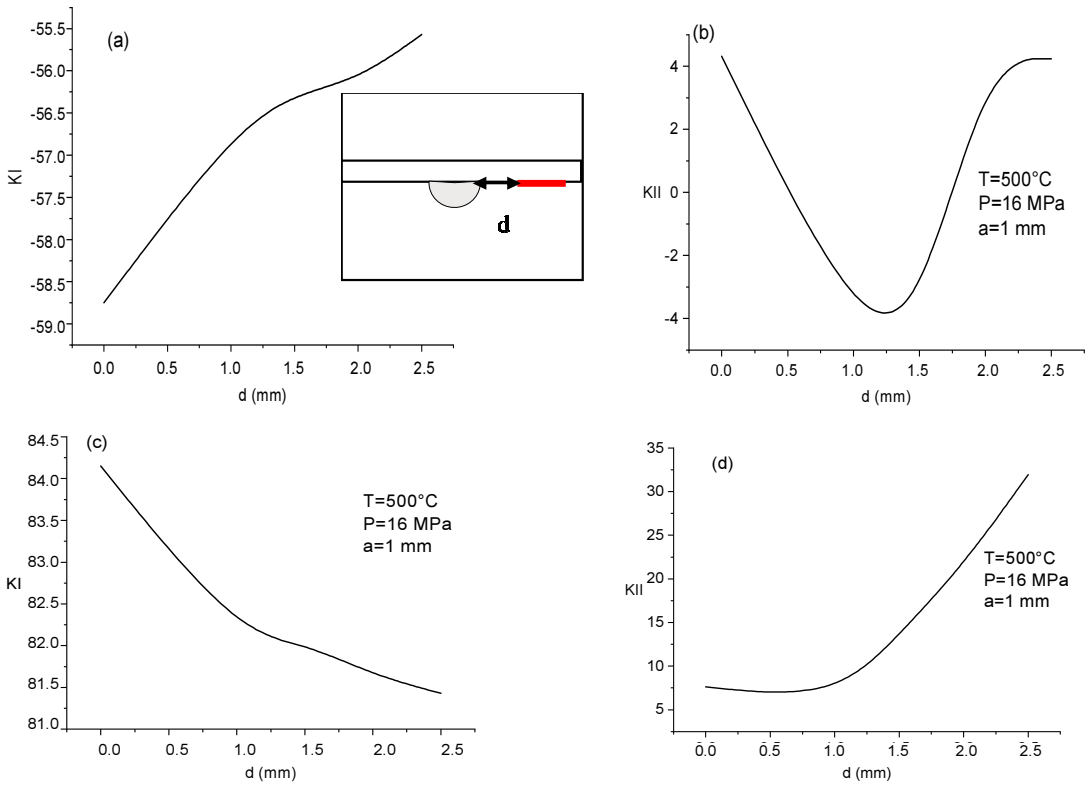

Fig. 12. Variation in stress intensity factor as function of crack-defect interaction along x-axis: a) Mode I in $Al_2O_3/Ni/Al_2O_3$, b) Mode II in $Al_2O_3/Ni/Al_2O_3$, c) Mode I in HAYNES^{TM}214/Ni/Al_2O_3, d) Mode II in HAYNES^{TM}214/Ni/Al_2O_3

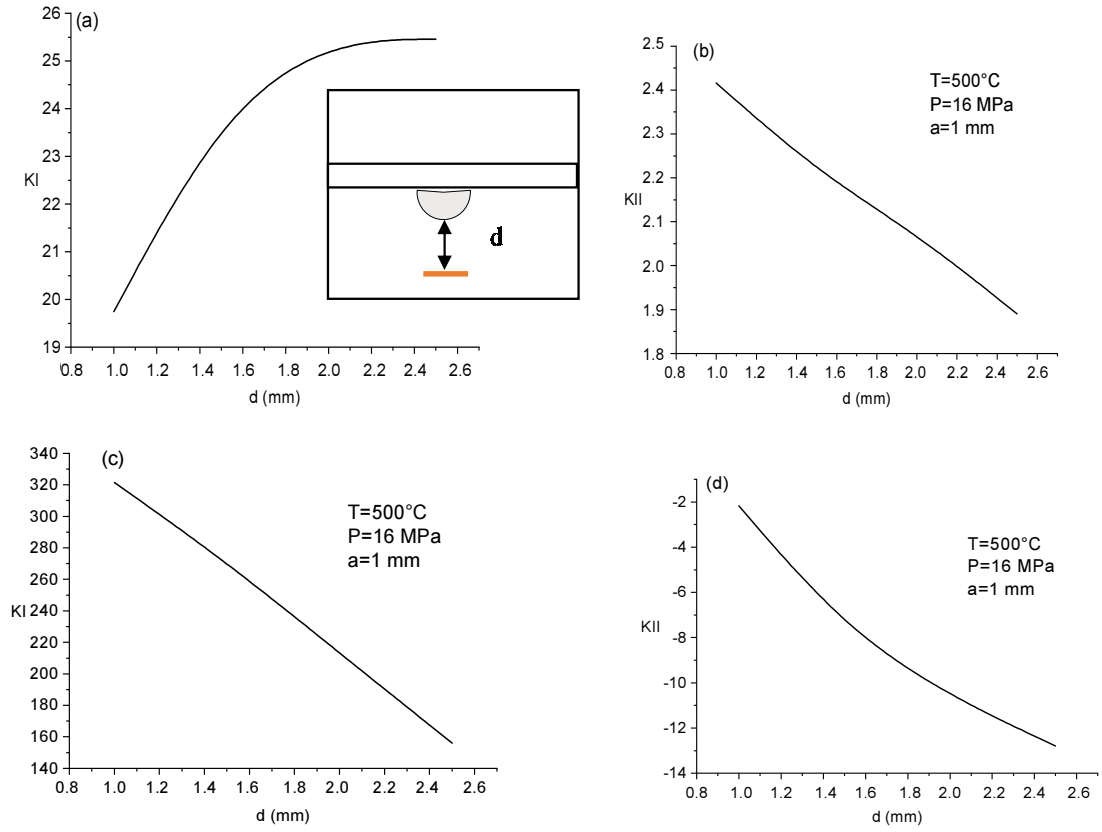

Fig. 13. Variation in stress intensity factor as a function of crack-defect interaction along y-axis: a) mode I in $Al_2O_3/Ni/Al_2O_3$, b) mode II in $Al_2O_3/Ni/Al_2O_3$, c) mode I in HAYNES^{TM}214/Ni/Al_2O_3, d) mode II in HAYNES^{TM}214/Ni/Al_2O_3

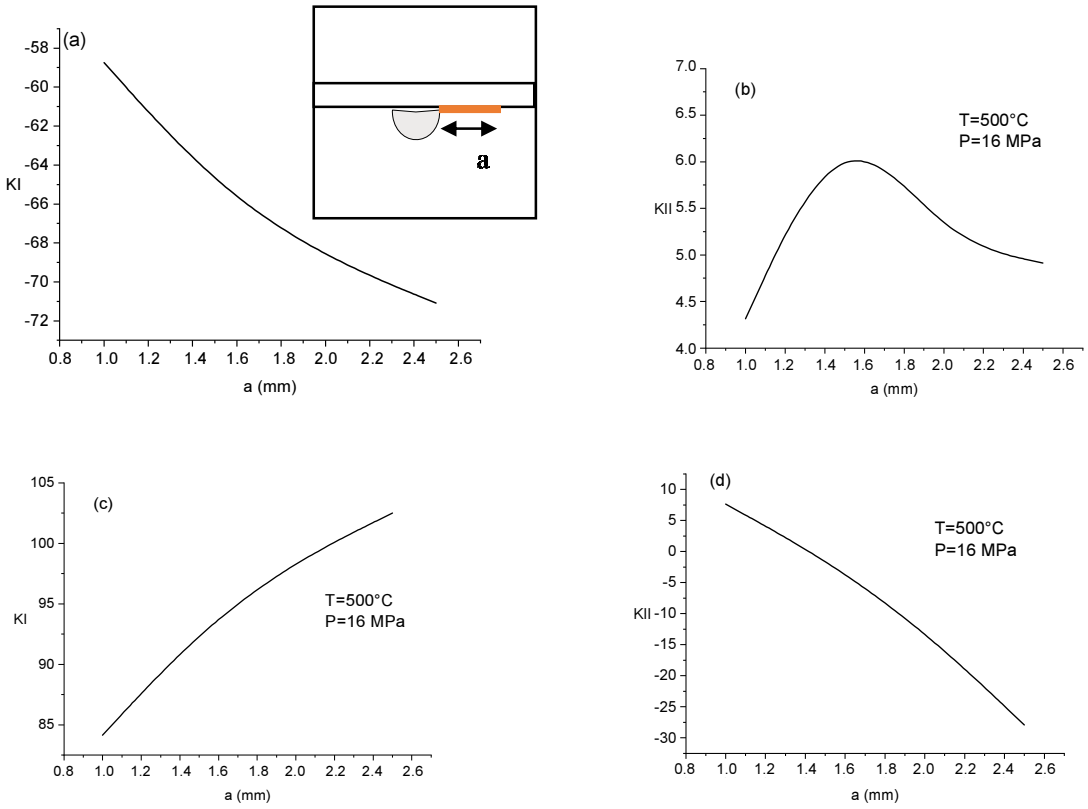

Fig. 14. Variation in stress intensity factor as a function of crack size along x-axis: a) mode I in $Al_2O_3/Ni/Al_2O_3$, b) Mode II in $Al_2O_3/Ni/Al_2O_3$, c) Mode I in HAYNES^{TM}214/Ni/Al_2O_3, d) Mode II in HAYNES^{TM}214/Ni/Al_2O_3

The variation in the stress intensity factor according to the size of the crack, which is located at the ceramic/metal interface, is shown in Figure 14. For both assemblies, the stress intensity factor values in Mode I rise as the size of the crack grows, except for the fact that SIF in the second assembly is higher (see Fig. 14c). SIF in Mode II for the $Al_2O_3/Ni/Al_2O_3$ assembly is negligible and unstable (see Fig. 14b), while in the second assembly, HAYNES^{TM}214/Ni/Al_2O_3, the intensity of SIF augments as the size of the crack increases (see Fig. 14d). The analysis of this figure clearly shows that the size of the crack significantly affects the stress intensity factor, especially in the second assembly.

CONCLUSIONS

The results obtained in this study allow the following conclusions to be drawn:

1. The interface is a site of stress concentration. The level and the distribution of normal and von Mises stresses depend on the bonding temperature; the assembly made at high temperatures induced more intense residual stresses. These stresses added to the applied mechanical stresses may present a risk of failure of the assembly.
2. The presence of this defect on the surface of the ceramic bonded to metal plays a leading role in the stress concentration, whose intensity grows with the increment in thermal loading of the bond.
3. The crack-interface defect has an effect on SIF; the presence of a crack near the interface defect increases the stress intensity factor (SIF) for Mode I. These parameters are more important in the HAYNES^{TM}214/Ni/Al_2O_3 assembly no matter where the crack exists; this indicates that the use of the alloy weakens the ceramic.
4. The stress intensity factor value in the symmetric assembly rises as the distance between the crack and the defect increases along the y-axis.
5. The size of the crack also affects the stress intensity factors; this parameter is higher as the size becomes bigger.
6. The stress intensity factors in Mode II for the symmetric assembly are almost negligible even if the crack changes size or direction, while this parameter in the HAYNES^{TM}214/Ni/Al_2O_3 assembly is more important, especially when the crack is at the interface.

REFERENCES

[1] Hadid L., Bouafia F., Serier B., Sikandar Hayat S., Finite element analysis of the interface defect in ceramic-metal assemblies: Alumina-silver, Frattura ed Integrita Strutturale 2020, 14(53), 1-12, DOI: 10.3221/IGF-ESIS.53.01.

[2] Ouinas D., Sahnoun M., Benderdouche N., FE analysis of SIF of interfacial crack emanating from a circular notch in ceramic/metal bi-materials, Advanced Materials Research 2012, 428, 121-126, DOI: 10.4028/www.scientific.net/AMR.428.121.

[3] Yi R., Chen C., Shi C., Li Y., Li H., Ma Y., Research advances in residual thermal stress of ceramic/metal brazes, Ceramics International 2021, 47(15), 20807-20820, DOI: 10.1016/j.ceramint.2021.04.220.

[4] Jin B., Huang X., Zou M., Zhao Y., Wang S., Mao Y., Joining of Al_2O_3 ceramic to Cu using refractory metal foil, Ceramics International 2022, 48(3), 3455-3463, DOI: 10.1016/j.ceramint.2021.10.123.

[5] Hafez K., El-Sayed M., Naka M., Joining of alumina ceramics to metals, Science and Technology of Welding and Joining 2005, 10(2), 125-130, DOI: 10.1179/174329305X19312.

[6] Zhang J.X., Chandel R.S., Chen Y.Z., Seow H.P., Effect of residual stress on the strength of an alumina – steel joint by partial transient liquid phase (PTLP) brazing, Journal of Materials Processing Technology 2002, 122(2-3), 220-225, DOI: 10.1016/S0924-0136(02)00010-9.

[7] Yang Z.W., Yang J.H., Han Y.J., Wang Y., Wang, D.P., Microstructure and mechanical properties of 17-4 PH stainless steel and Al_2O_3 ceramic joints brazed with graphene reinforced Ag-Cu-Ti brazing alloy, Vacuum 2020, 181(July), 109604, DOI: 10.1016/j.vacuum.2020.109604.

[8] Lourdin P., Juvé D., Tréheux D., Nickel-alumina bonds: mechanical properties related to interfacial chemistry, Journal of the European Ceramic Society 1996, 16(7), 745--752, DOI: 10.1016/0955-2219(95)00187-5.

[9] Huh S.C., Park W.J., Park S.H., Evaluation of design strength and residual stress in ceramic/metal joint, JSME International Journal, Series A: Solid Mechanics and Material Engineering 2006, 49(1), 48-52, DOI: 10.1299/jsmea.49.48.

[10] Hattali M.L., Valette S., Ropital F., Mesrati N., Tréheux D., Interfacial behavior on Al_2O_3/HAYNES® 214™ joints fabricated by solid state bonding technique with Ni or Cu-Ni-Cu interlayers, Journal of the European Ceramic Society 2012, 32(10), 2253-2265, DOI: 10.1016/j.jeurceramsoc.2012.01.036.

[11] Kovalev S.P., Miranzo P., Osendi M.I., Finite element simulation of thermal residual stresses in joining ceramics with thin metal interlayers, Journal of the American Ceramic Society 1998, 81(9), 2342-2348, DOI: 10.1111/j.1151-2916.1998.tb02630.x.

[12] Feng Q., Lin P., Ma G., Lin T., He P., Long W., Zhang Q., Design of multi-layered architecture in dissimilar ceramic/metal joints with reinforcements clustering away from both substrates, Materials and Design 2021, 198, 109379, DOI: 10.1016/j.matdes.2020.109379.

[13] Vila M., Prieto C., Zahr J., Pérez-Castellanos J.L., Bruno G., Jiménez-Ruiz M., Miranzo P., Osendi M.I., Residual stresses in ceramic-to-metal joints: Diffraction measurements and finite element method analysis, Philosophical Magazine 2007, 87(35), 551-5563, DOI: 10.1080/14786430701673436.

[14] Ramdoum S., Bouafia F., Serier B., Fekirini H., Effect of residual stresses on the stress intensity factor of cracks in a metal matrix composite: Numerical analysis, Mechanics and Mechanical Engineering 2018, 22(1), 119-131, DOI: 10.2478/mme-2018-0011.

[15] Cazajus V., Lorrain B., Welemane H., Karama M., Residual stresses in ceramic metal assembly after brazing process, Advances in Science and Technology 2006, 45, 1543-1550, DOI: 10.4028/www.scientific.net/ast.45.1543.